Chaos
An Interdisciplinary Journal of Nonlinear Science

RESEARCH ARTICLE | MAY 01 2023

Study of turbulent transport in magnetized plasmas with flow using symplectic maps

Jorge Torres; Julio J. Martinell

Chaos 33, 053102 (2023)
https://doi.org/10.1063/5.0144037

Study of turbulent transport in magnetized plasmas with flow using symplectic maps

Cite as: Chaos **33**, 053102 (2023); doi: 10.1063/5.0144037
Submitted: 27 January 2023 · Accepted: 3 April 2023 ·
Published Online: 1 May 2023

Jorge Torres and Julio J. Martinell[a)]

AFFILIATIONS

Instituto de Ciencias Nucleares, UNAM, A. Postal 70-543, México City, Mexico

[a)]**Author to whom correspondence should be addressed:** martinel@nucleares.unam.mx

ABSTRACT

Turbulent transport in a magnetized plasma of the kind found in tokamaks is modeled by a 2D wave spectrum that allows reduction to a symplectic map. The properties of particle transport when chaos sets in are analyzed in various circumstances including finite Larmor radius (FLR) effects and a background plasma flow. For large wave amplitudes, regular particle orbits become chaotic, which represents a type of Lagrangian turbulence. When chaos becomes global, it leads to the loss of particle confinement. Poloidal flows tend to decrease the chaos in some regions, and they can give rise to the formation of transport barriers. FLR effects not only reduce chaos but also give rise to non-local behavior. Thus, when the particles have a thermal distribution of Larmor radii, a non-Gaussian particle distribution function in space is obtained. However, the transport preserves its diffusive scaling when there is no flow. Previous results about the dependence of the diffusion coefficient with amplitude are re-derived analytically and numerically taking into account FLR effects. In the presence of general poloidal flows, the transport has to be described by a two-step map. They modify the nature of transport in the direction of the flow from diffusive to ballistic to super-ballistic, depending on the type of flow. The transverse transport, in turn, shows suppression of the oscillations with wave amplitude that are present in the absence of flow. When the plasma flow varies linearly with radius, the transport can be studied with a similar single-step map, and the transverse diffusion coefficient is reduced while parallel transport can become super-ballistic. For non-monotonic flows, there are accelerating modes that can produce ballistic-like particles while the bulk of the particles behaves diffusively.

Drift wave turbulence is thought to be responsible for anomalous transport in magnetized plasmas, but its study is complicated. Simple models have been developed that describe particle motion in the wave fields that can be reduced to the use of mappings. They can describe weak turbulence transport. In this way, some properties of transport can be studied based on the chaotic nature of the maps. The presence of transport barriers often seen in plasmas can be identified with the resilience of Kolmogorov-Arnold-Moser (KAM) surfaces in the transition to chaos, which occurs when there is a sheared background flow present. In this work, we study the statistical properties of the maps in various circumstances that include no flow, monotonic, and non-monotonic shear flow. The effect of a finite Larmor radius (FLR) is explored both for a fixed radius and for a thermal distribution of Larmor radii. We focus on the type of transport resulting in each case being diffusive, super-diffusive, ballistic, or even super-ballistic. Also, we describe the probability distribution functions (PDFs) in each situation finding that, as a rule, they become non-Gaussian when there is a thermal distribution of FLR with high temperature. The PDF has exponentially decaying tails which tells us that non-local features are introduced. Our study includes analytical derivations of results as well as numerical computations which agree quite well and help to understand the nature of the phenomena involved.

I. INTRODUCTION

Transport in magnetically confined plasmas due to turbulence is a very complex process, which is usually studied with numerical codes based on gyro-kinetic models or particle-in-cell methods. However, an important insight can be gained with simpler models that analyze the interaction of particles with a certain wave spectrum representing the turbulent fluctuations, which are usually due to unstable drift waves. The resulting cross field particle transport is what determines the plasma confinement time in fusion experiments. The wave–particle interaction for a test particle, which does not affect the background fields, can be used as an indicator

of what plasma particles will experience in this turbulent field. For electrostatic turbulence in a magnetized plasma, the gyrating charged particles would experience a drift dominated mostly by the $E \times B$ velocity. Thus, the particle motion to the lowest order can be described using the guiding center approximation if the electric fields produced by the electrostatic turbulence are given. With this description, the particle trajectories can be studied using a Hamiltonian approach once the spectrum of drift waves is provided.[1,2] Naturally, the type of wave spectrum is determinant for the resulting particle trajectories.

In fusion experiments, the presence of macroscopic plasma flows is quite common, and this effect can be incorporated by introducing also large-scale electric fields perpendicular to the B field and the flow direction. In particular, in toroidal configurations, a radial electric field gives rise to the poloidal flows that are usually observed. When the flow has a radial shear, it is known to have a stabilizing effect on turbulence. Thus, using the $E \times B$ approach, the simultaneous action of waves and flows can be studied. A very simple case of wave–particle interaction studied using this approach was undertaken in Refs. 3 and 4, where just two waves with different phase velocities were considered in the presence of a poloidal zonal flow. This can retain the basic nonlinearities and allows studying the conditions for the establishment of global chaos identified with turbulent transport.

When the particle Larmor radius is not small compared to the characteristic plasma scales, the guiding center approximation is not good enough since the fields that the particles feel can be quite different from those at the center of the orbit. This problem can be solved by taking an average over the gyro-orbit finite Larmor radius. It has been shown that inclusion of finite Larmor radius effects (FLR) in this way gives rise to reduction of the chaotic transport region,[4] which implies that high energy particles (like the fusion reaction products), which have large Larmor radii, would be lost at a slower rate than thermal particles.

The Hamiltonian model has been used previously in various studies in plasmas and fluids,[1,5] providing an understanding of the basic physical processes. The main feature is that wave–particle interactions give rise to deterministic chaos of the particle orbits (interpreted as Lagrangian turbulence), but, this chaos can be substantially modified by sheared flows as observed for instance in geostrophic fluids, as studied in Ref. 5, which considered the zonal flows concentrated in latitude leading to suppression of cross-flow transport. In the Hamiltonian description, the transport suppression is identified with a surface in phase-space that is resilient to chaos located around the maximum of the velocity profile where the shear vanishes (the so-called shearless curve).[2] This is also called a transport barrier and remains unbroken until the wave amplitude is large enough. Zonal flows in fusion plasmas usually refer to a more complex process involving self-generated flows by the turbulence itself, but here we consider that a zonal flow is simply a given radially localized poloidal flow and independent of poloidal and toroidal angles since we do not deal with a self-consistent study. Thus, a poloidal velocity profile with a non-monotonic radial variation is identified with a zonal flow.

The specific type of wave spectrum considered here is such that the equations of motion can be reduced to an iterative mapping. It contains an infinite number of waves in two dimensions propagating in the poloidal direction with a uniform distribution of discrete frequencies. This in some sense generalizes the two-wave spectrum studied previously.[4] In the absence of flows, this particular choice of waves was used to derive a symplectic mapping in Ref. 1 and show the resulting chaotic transport. The statistical properties of an ensemble of particles governed by the map followed for a period of time lead to derive a diffusion coefficient that is proportional to the square of the wave amplitude. FLR effects were included in Ref. 2 showing that under certain conditions the transport can become non-diffusive. In this work, we show that when macroscopic flows are included, particle orbits have to be described in general by two-step maps. In the language of mapping theory, monotonic flows produce twist maps while non-monotonic flows give rise to non-twist maps.

The aim of the present paper is to extend the study of the properties of the Karney map[6] reported previously[1,7] to cases including FLR and two types of plasma flows, monotonic and non-monotonic. We focus on the statistical properties of chaotic transport, when regular orbits are destroyed. We show that taking a thermal distribution of Larmor radii gives rise to particle distribution functions (PDF) that are non-Gaussian, not only for the cases without flow[2] but also when a flow of any kind is present. We also find that the oscillatory dependence of the diffusion coefficient D with the wave amplitude A[7] around the quasilinear value is preserved for localized non-monotonic flows, but it gets smoothed out for the unlimited monotonic flow. In addition, the oscillations get translated to the dependence with Larmor radius acquiring a double oscillation.

The paper is organized as follows. In Sec. II, the test particle model used is described in the $E \times B$ approximation and the corrections due to FLR are introduced. The representation of the waves is described leading to the iterative mapping for the particle evolution. The properties of the map without macroscopic flow are described in Sec. III noting that the effect of FLR is to reduce the chaotic regions in the particle trajectories and to create non-Gaussian PDF when Larmor radii have a Maxwellian distribution. Then, in Sec. IV, a macroscopic poloidal flow is included giving rise to a two-step map; its properties are studied first for a flow that is linearly increasing in the radial direction. FLR effects are introduced and the statistical behavior is analyzed for transport in both directions. Also, the effect of a thermal distribution of particles is described; it is noted that the transport parallel to the flow can become super-ballistic, but it becomes only super-diffusive when the velocity is kept finite at large distances (as for a radially limited flow). Section IV B analyzes the effect of a non-monotonic flow that has a maximum at a given radial position. For a flow with a Gaussian radial profile, the transport in radial and poloidal directions is studied. Here, the FLR gyro-averaging has to be done numerically as well as the inclusion of a thermal distribution of Larmor radii. Finally, the conclusions and a discussion of results are presented in Sec. V.

II. TEST PARTICLE MODEL

The $\mathbf{E} \times \mathbf{B}$ guiding center velocity for a particle in a magnetized plasma gives the lowest order motion in the presence of electrostatic fields, which can be large-scale quasistatic or small scale fluctuating. The equations of motion provide the time evolution equation for the guiding center position as

$$\frac{d\mathbf{r}}{dt} = \frac{\mathbf{E}\times\mathbf{B}}{B^2}.$$

Taking the uniform magnetic field as an approximation (the toroidal field in a tokamak, for instance), $\mathbf{B} = B_0\hat{\mathbf{z}}$, we can focus on the perpendicular motion since the velocity along the field is constant. Then, $\mathbf{r} = (x, y)$ is the test particle guiding center position in 2D, where x can be identified with the radial coordinate and y with the poloidal coordinate. In terms of the electrostatic potential defined by $\mathbf{E} = -\nabla\phi(x, y, t)$, the equation has the structure of a Hamiltonian dynamical system with $H = \phi$,

$$\frac{dx}{dt} = -\frac{\partial\phi}{\partial y}, \qquad \frac{dy}{dt} = \frac{\partial\phi}{\partial x}, \tag{1}$$

where x and y are the canonically conjugate variables.

The approximation of zero Larmor radius is not good for energetic particles since the fields the particle samples in an orbit can be quite different from those at the guiding center. Finite Larmor radius (FLR) is taken into account by averaging the equations over the gyro-orbit,

$$\frac{dx}{dt} = -\left\langle\frac{\partial\phi}{\partial y}\right\rangle_\theta, \qquad \frac{dy}{dt} = \left\langle\frac{\partial\phi}{\partial x}\right\rangle_\theta \tag{2}$$

where the average, for the Larmor radius ρ, is defined as

$$\langle\Psi\rangle_\theta \equiv \frac{1}{2\pi}\int_0^{2\pi}\Psi\left(x+\rho\cos\theta, y+\rho\sin\theta\right)d\theta. \tag{3}$$

Following the approach in Ref. 2, the wave spectrum is assumed to have a wide distribution with an infinite number of waves having the same wavenumber and amplitude A, given by

$$\phi = A\sum_{n=-\infty}^{\infty}\cos(x+\theta_n)\cos(y+\theta_n-nt). \tag{4}$$

Using the identity for the Fourier representation of the delta function, $\sum_{n=-\infty}^{\infty}\cos(nt) = 2\pi\sum_{m=-\infty}^{\infty}\delta(t-2\pi m)$, the equations of motion in terms of the new variables $x_\pm = x \pm y$ reduce to[1]

$$\frac{dx_+}{dt} = -2\pi A\sum_{m=-\infty}^{\infty}\sin(x_-)\delta(t-2\pi m),$$

$$\frac{dx_-}{dt} = 2\pi A\sum_{m=-\infty}^{\infty}\sin(x_+)\delta(t-(2m+1)\pi).$$

This can be expressed as a two-step map

$$\begin{aligned} x_+(t_{2m}^+) &= x_+(t_{2m}^-) - 2\pi A\sin(x_-(t_{2m}^-)),\\ x_-(t_{2m}^+) &= x_-(t_{2m}^-),\\ x_+(t_{2m+1}^+) &= x_+(t_{2m+1}^-),\\ x_-(t_{2m+1}^+) &= x_-(t_{2m+1}^-) + 2\pi A\sin(x_+(t_{2m+1}^+)), \end{aligned} \tag{5}$$

where $t_{2m}^\pm$ denote time at $2m\pi$ just before $(-)$ and just after $(+)$ the delta-function jump. This map first produces a displacement along the line $x - y =$ const. and in the second step it displaces along the line $x + y =$ const. Identifying t_{2m}^+ with t_{2m+1}^-, it can be reduced to a one-step map

$$\begin{aligned} x_+^{n+1} &= x_+^n - 2\pi A\sin(x_-^n),\\ x_-^{n+1} &= x_-^n + 2\pi A\sin(x_+^{n+1}). \end{aligned}$$

Notice that this iterative map is exact and totally equivalent to solving the differential equations since no discretization has been applied.

After gyro-averaging, it takes the form

$$\begin{aligned} x_+^{n+1} &= x_+^n - 2\pi AJ_0(\sqrt{2}\rho)\sin(x_-^n),\\ x_-^{n+1} &= x_-^n + 2\pi AJ_0(\sqrt{2}\rho)\sin(x_+^{n+1}), \end{aligned} \tag{6}$$

where $J_0(x)$ is the Bessel function of zero order.

The map (6) was found in Ref. 6, and it has been already studied in detail in Ref. 2. Here, we only present the phase-space structure of the particle orbits for reference. Figure 1 shows the orbits with practically no chaos for a low amplitude wave $A = 0.01$ and $\rho = 0$, then

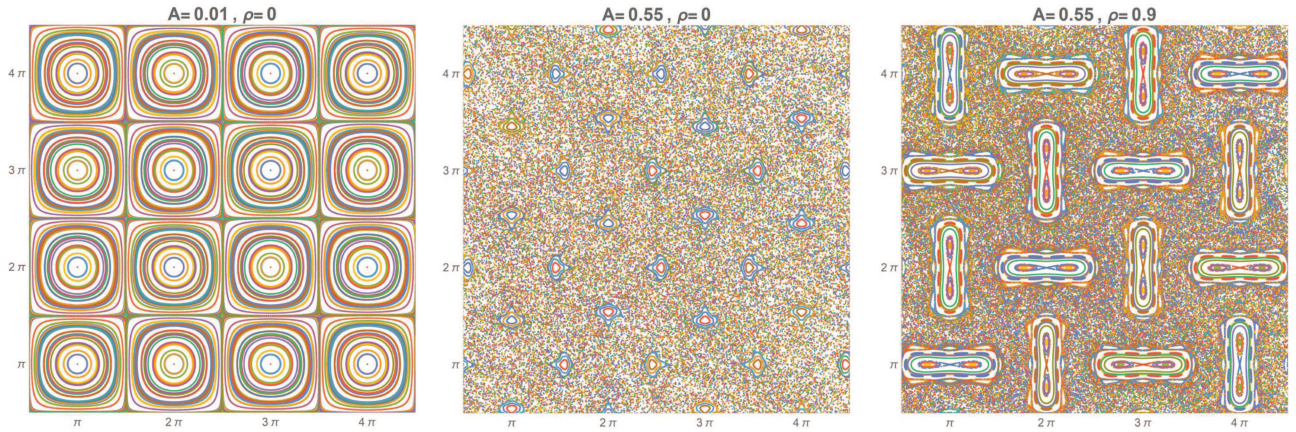

FIG. 1. Phase-space diagram for the particle orbits with $A = -0.01$, $\rho = 0$ (left), $A = -0.55$, $\rho = 0$ (middle), and $A = -0.55$, $\rho = 0.9$ (right).

when chaos is prevalent for $A = 0.55$ and still $\rho = 0$ and, finally, the chaos reduction effect of FLR for $A = 0.55$, $\rho = 0.9$. The later property implies that particles with larger Larmor radius are less chaotic and are thus better confined.

III. TRANSPORT WITH NO PLASMA FLOW

To study particle transport an ensemble of particles is initialized in a small region centered at $x = y = 0$. It is followed in time and the moments of the particle distribution are taken in order to analyze the type of transport that results. When the wave amplitude is kept small, there is practically no transport since particles stay is closed orbits. As A increases chaos becomes more extended and the particles experience diffusion. For the validity of statistical analysis, the phase space has to be chaotic globally which typically happens for $A \geq 1$. This was shown in Ref. 2. The transport is diffusive because the variance of the distribution function scales linearly with time: $\sigma^2 = \langle x^2 \rangle \sim t$. The proportionality constant is the diffusion coefficient, which can be computed analytically and is given by the so-called quasilinear diffusion coefficient[1]

$$D = \pi^2 A^2/2 \equiv D_{ql}. \tag{7}$$

In deriving this expression, it is assumed that there is no correlation between successive iterations. This has the characteristic A^2 scaling and can be tested numerically by fitting D vs A^2 with a straight line. The diffusive nature of transport is also verified numerically by fitting a straight line to σ^2 vs t. It is known[8] that corrections to D_{ql} due to correlations between successive steps produce oscillations with A, which, in this case, are given by[7]

$$D = \pi^2 A^2/2(1 + 2J_0(2\pi A) + 0(A^{-1})). \tag{8}$$

The numerical check of this expression is presented in Fig. 2. Exploring other statistical properties of the transport one finds that the particle distribution function (PDF) for a given time is a Gaussian whose width increases linearly with time. This is true for both x and y directions since the map is symmetrical in these variables; then, $D_x = D_y = D$.

Now, when FLR effects are included by applying the map of Eq. (6), similar results are obtained just making the substitution $2\pi A \to A(\rho) = 2\pi A J_0(/\sqrt{2}\rho)$. This implies that the diffusion coefficient presents oscillations with ρ due to the Bessel function. The quasilinear value is $D_{\rho ql} = \pi^2 A^2 J_0^2(\sqrt{2}\rho)$, while the complete diffusion coefficient D_ρ corresponding to Eq. (8) has a double oscillation. This is corroborated by the numerical results as shown in Fig. 3 where the agreement is very good.

Since in a plasma the particles have different velocities, given by a distribution function, the Larmor radii of the particle ensemble should also not be the same for all particles. Then, we can take the initial ρ with a distribution which for a thermal plasma is a Maxwellian. Given that we are following the dynamics in the plane perpendicular to the magnetic field the radii distribution is a 2D Maxwellian

$$f_{th}(\rho) = \left(2\rho/\rho_{th}^2\right) \exp\left[-(\rho/\rho_{th})^2\right]. \tag{9}$$

When this initial distribution is taken there are two interesting effects. The transport is still diffusive [i.e., $\sigma^2 \sim t$] with a diffusion coefficient that has practically no oscillations and the PDF is not necessarily Gaussian, but it can have long tails that decay exponentially for large x. The latter is an indication that the transport is non-local. The diffusion coefficient can be obtained analytically using a probability distribution given by the average of the Gaussian PDFs, $f_\rho(x,t) = (4\pi D_\rho t)^{-1/2} e^{-x^2/4D_\rho t}$ weighted by the distribution of Larmor radii, Eq. (9),

$$P(x,t) = \int_0^\infty f_{th}(\rho) f_\rho(x,t) d\rho. \tag{10}$$

The variance is obtained by taking the second moment of $P(x,t)$, which follows the scaling $\sigma^2 \sim t$, and the proportionality constant is the diffusion coefficient, which is found to be

$$\langle D \rangle = D_{ql}\left[e^{-\rho_{th}^2} I_0(\rho_{th}^2) + \int_0^\infty \frac{4\rho}{\rho_{th}^2} e^{-\left(\frac{\rho}{\rho_{th}}\right)^2} J_0^2(\sqrt{2}\rho) J_0(2\pi A J_0(\sqrt{2}\rho)) d\rho\right]. \tag{11}$$

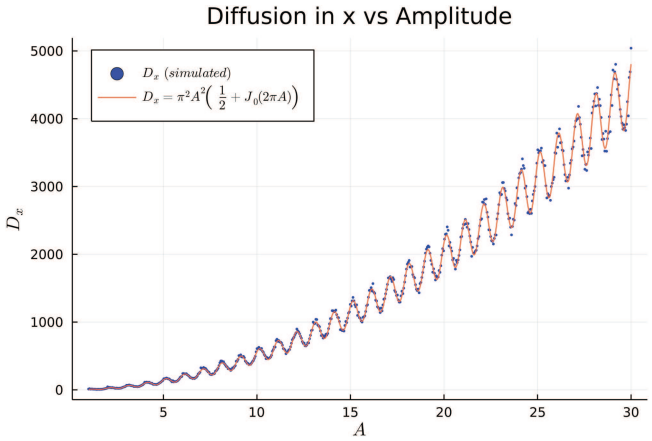

FIG. 2. Oscillations in the diffusion coefficient with wave amplitude A.

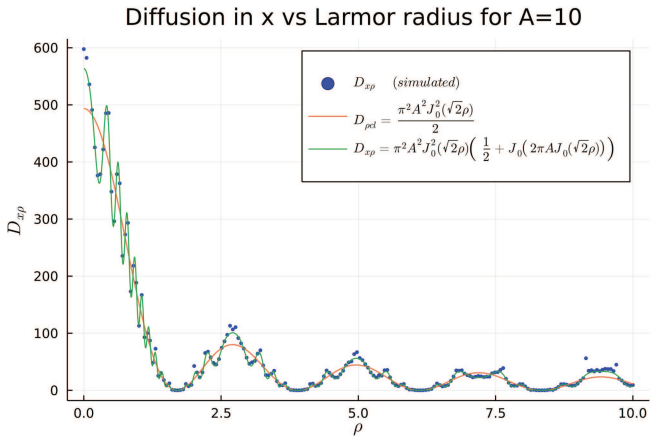

FIG. 3. Oscillations in the diffusion coefficient with Larmor radius ρ.

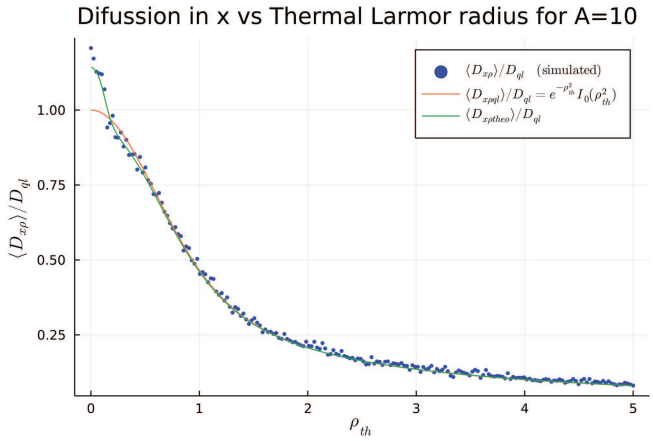

FIG. 4. Thermally averaged diffusion coefficient for amplitude $A = 10$ normalized to the 0th order value, $D_0 \equiv D_{ql}$, compared with numerical values. The quasilinear approximation, in red, fits well the results for all but the lowest values of ρ_{th}.

The first term is actually the thermal average of the quasilinear diffusion coefficient $\langle D_{\rho ql}\rangle$. In Fig. 4, this expression is plotted together with the results of numerical simulations. The quasilinear thermal coefficient is also plotted for comparison. It can be seen that the match is very good even for the quasilinear estimate, differing only for very small thermal radius. An interesting feature is that $\langle D_\rho\rangle$ decreases with ρ_{th}, which implies that hotter plasmas have less diffusion than cooler plasmas.

The PDF of Eq. (10) can be shown to have a non-Gaussian dependence for large ρ_{th}. In particular, it has the asymptotic limits

$$P(\xi, \rho_{th} \to 0) = \frac{1}{\sqrt{2\pi}} e^{-\xi^2/2}, \tag{12}$$

$$P(\xi, \rho_{th} \gg 1) \approx \frac{a}{2} e^{-a|\xi|}, \tag{13}$$

where $\xi = x/\sqrt{2\langle D\rangle t}$ is a self-similarity variable and a is a function of ρ_{th}. In terms of the variable ξ, the PDF turns out to be self-similar,

$$P(x,t) = \frac{1}{\sqrt{2\langle D\rangle t}} \mathscr{G}_{\rho_{th}}(\xi), \tag{14}$$

where $\mathscr{G}_{\rho_{th}}$ is a function determined by the thermal Larmor radius. These properties are presented in Fig. 5, where PDFs for different times and wave amplitudes collapse to the same function which, in turn, changes from a Gaussian to another having exponential tails for large ρ_{th}. Thus, transport in a thermal hot plasma has the interesting property of being diffusive but non-local.

IV. PRESENCE OF POLOIDAL FLOWS

When a macroscopic poloidal flow along y is included the potential ϕ has to be modified by adding a function of x, $\phi_0(x)$ representing a radial electric field (i.e., replace $\phi(x,y) \to \phi_0(x) + \phi(x,y)$). It turns out that in this case, the two-step map [Eq. (5)] cannot be reduced to a one-step map in general. The resulting two-step map is

$$\begin{aligned} x_-^{n+\frac{1}{2}} &= x_-^n - \pi\,\Omega(x^n), \\ x_+^{n+\frac{1}{2}} &= x_+^n - 2\pi A J_0\left(\sqrt{2}\rho\right) \sin\left(x_-^{n+\frac{1}{2}}\right) + \pi\,\Omega(x^n), \\ x_+^{n+1} &= x_+^{n+\frac{1}{2}} + \pi\,\Omega\left(x^{n+\frac{1}{2}}\right), \\ x_-^{n+1} &= x_-^{n+\frac{1}{2}} + 2\pi A J_0\left(\sqrt{2}\rho\right) \sin\left(x_+^{n+1}\right) - \pi\,\Omega\left(x^{n+\frac{1}{2}}\right), \end{aligned} \tag{15}$$

where $\Omega(x) = \phi_0'(x)$ is the gyroaveraged flow velocity profile. Depending on the type of function chosen for $\Omega(x)$, the map can have different properties. In particular, when $\Omega(x)$ is a monotonic function it produces a twist map, while for a non-monotonic function the result is a non-twist map.

A. Linear shear flow

When $\Omega(x)$ is linear the map (15) has a non-zero Jacobian everywhere which implies that this is a twist map. Writing $\Omega(x) = Cx$ the strength of the shear flow is measured by C. A simpler one-step map can be proposed when the flow is linear in x,[2] although it is not strictly derived from the integration of the equations of motion. However, it can be used to derive some properties of transport analytically. It is actually an implicit map but when converted to an explicit mapping, it takes the form[2]

$$\begin{aligned} x_+^{n+1} &= x_+^n - 2\pi A J_0\left(\sqrt{2}\rho\right) \sin(x_-^n) + \frac{C}{2}\left(x_+^n + x_-^n\right), \\ x_-^{n+1} &= \frac{1}{1+C/2}\left[x_-^n + 2\pi A J_0\left(\sqrt{2}\rho\right) \sin\left(x_+^{n+1}\right) - \frac{C}{2} x_+^{n+1}\right]. \end{aligned} \tag{16}$$

The phase-space structure for this one-step map has been discussed in Ref. 2. With the flow, the first thing to notice is that closed orbits are mostly stretched to form open orbits. These streamlines actually play the role of invariant tori in the Hamiltonian system. They start to break up as the amplitude A increases giving way to chaos and the most robust of the torii act as transport barriers. In the two-step map, the phase-space looks a little different, but it has essentially the same properties.

In the presence of flow, the symmetry in x and y is broken and the transport in each direction has to be considered separately. It is clear that transport along the flow direction is not hindered by transport barriers and particles can always be moving along the y direction. However, transport along the x direction is only important when there are no transport barriers anymore. Here, we will not focus on how the barriers break up, which was considered in Ref. 9 but assume the condition of global chaos is fulfilled when transport in the x direction is studied.

1. Transport in x direction

In order to describe the type of transport involved, we computed the variance of the ensemble of particles as function of time (or equivalently, the iteration number n), and the result is fitted by a

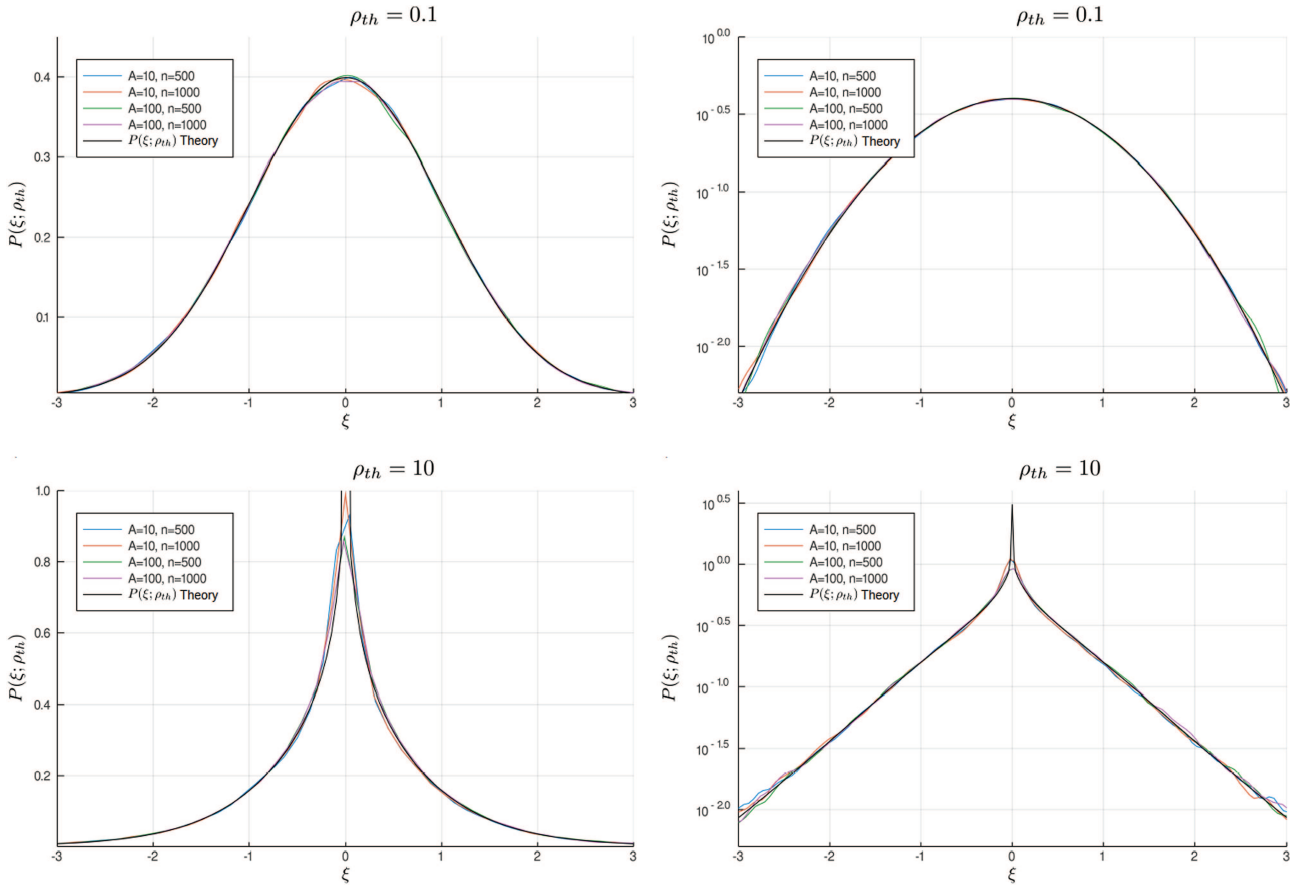

FIG. 5. PDF in linear and semi-log scales showing the transition from Gaussian to exponential decay when ρ_{th} is increased from 0.1 to 10. Plots for different values of A and time (number of iterations n) show the self-similar behavior, in agreement with theoretical prediction.

power law

$$\sigma_x^2 = T_x n^{\gamma_x}. \tag{17}$$

As before, the simulation starts an ensemble of particles (4000 in this case) in a small square of size 10^{-5} around a hyperbolic point and is evolved for 5000 iterations. In order to have a statistically representative database, in computing Eq. (17), A was made to vary over 600 values uniformly distributed. It was found that $\gamma_x = 1.0 \pm 0.01$ meaning that the transport is diffusive. Thus, the coefficient T_x is the diffusion coefficient D_x but in this case, when taken as a function of the wave amplitude it does not show the oscillations observed without flow. It rather approximately follows the quasilinear scaling as seen in Fig. 6. It is apparent that the flow has the effect of almost vanishing the correlations between successive steps and smoothing the function $D_x(A)$. Regarding the PDF, it is still a Gaussian as in the case with no flow.

The diffusion associated with this system is not easy to study analytically with the two-step map but using the similar one-step map an analytical expression can be derived[2] for the modified quasilinear diffusion coefficient

$$D_x(\rho) = \frac{1}{2(1+C/2)^2}\left(\pi A J_0\left(\sqrt{2}\rho\right)\right)^2, \tag{18}$$

which shows that diffusion is reduced by the flow. This is expected to be different for the two-step map but the effect of transport reduction would be the same.

a. FLR effects. The process of gyro-averaging the equations produces similar effects on the transport along the x direction as in the case with no flow, in particular, the oscillations of D_x with ρ. Allowing now for a thermal distribution of Larmor radii, the result is to produce a non-Gaussian PDF for large ρ_{th}, as in the case without flow, as was shown in Ref. 2. In addition, the PDF is self-similar in the same way as in the case with no flow, according to Eq. (14).

2. Transport in the y direction

For this case, transport is in the same direction as the flow and, therefore, it is very much affected by it. Following the same procedure to fit the variance to

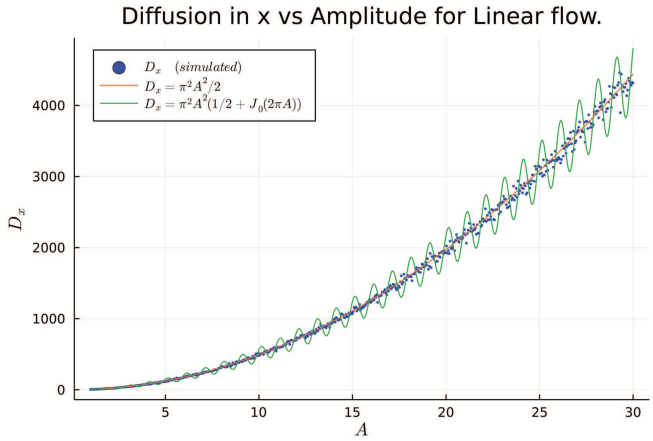

FIG. 6. Diffusion coefficient in the x direction for a linear flow with $C = 1$ spanning all x range as a function of A. It almost follows the quasilinear value (red line) and does not show oscillations as it was the case when no flow was present, which is shown by the green line.

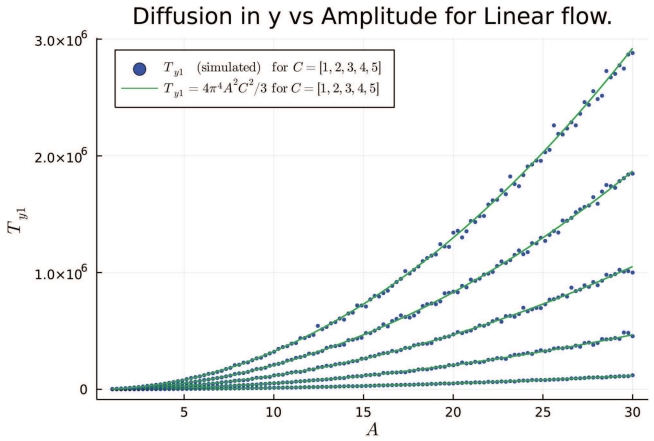

FIG. 7. Super-ballistic transport coefficient as a function of A for velocity shear values $C = 1, 2, 3, 4, 5$.

$$\sigma_y^2 = T_y n^{\gamma_y}. \tag{19}$$

It is now found that $\gamma_y = 3.01 \pm 0.01$, which means that the transport is super-ballistic. As explained in Ref. 2, this is due to the combined effect of diffusion in the x direction with the almost ballistic motion along y whose velocity is ever increasing with x. So, particles that manage to diffuse in x to distant positions are the ones that dominate the transport and give rise to the super-ballistic scaling. In order to have a better understanding of this effect and compute the variance to the lowest order, we can study a simplified map that preserves the essential features and is more tractable. This considers diffusion in the x direction and a linear flow in the y direction, i.e., the diffusion in y is not included. Thus, we consider the map

$$x^{n+1} = x^n + \chi^n, \tag{20}$$

$$y^{n+1} = y^n + 2\pi C x^n, \tag{21}$$

where χ^n is a random variable with normal distribution centered at zero and standard deviation σ. One can show that the variance of y for this map after n iterations is

$$\langle y^2 \rangle = 4\pi^2 C^2 \sigma^2 \frac{n(n+1)(2n+1)}{6} \to \frac{4\pi^2 C^2 \sigma^2}{3} n^3, \tag{22}$$

for large n. Therefore, this gives directly the super-ballistic scaling mentioned above.

For the x direction, it is straightforward to show that $\langle x^2 \rangle = \sigma^2 n$ and, thus, the corresponding diffusion coefficient would be $D_x = \langle x^2 \rangle / 2n = \sigma^2/2$. Since we know that $D_x = \pi^2 A^2/2$, this gives a relationship between σ and A which, when substituted in Eq. (22) for the variance, gives

$$\sigma_y^2 \equiv \langle y^2 \rangle = \frac{4\pi^4 C^2 A^2}{3} n^3. \tag{23}$$

This gives a transport coefficient for super-ballistic (not diffusive) transport, T_{y1} to first order, according to Eq. (19),

$$T_{y1} = \frac{4\pi^4 C^2 A^2}{3}. \tag{24}$$

In Fig. 7, we plot this coefficient against A for five values of the velocity $C = 1, 2, 3, 4, 5$ and compare with the corresponding simulations to check its accuracy, noting the good fit. Now, if the diffusive transport in the y direction that was ignored in this simplified map is added, it would contribute an extra term to σ_y^2, leading to

$$\sigma_y^2 = 2D_y n + T_{y1} n^3, \tag{25}$$

this is clearly dominated by the second term for large times leading to the super-ballistic transport that is observed.

There is also a self-similarity property for the PDF, which is a Gaussian function whose width varies as $t^{3/2}$

$$P(y, t) = \frac{1}{\sqrt{2\pi T_{y1} t^3}} e^{-\xi^2/2}, \tag{26}$$

with the self-similar variable $\xi = y/\sqrt{T_{y1} t^3}$. With this variable all the PDFs collapse to the same normal distribution.

At this point, it is relevant to notice that the linear velocity profile is not physical since the velocity tends to infinity as $|x| \to \infty$ and, therefore, the super-ballistic scaling is not realistic. A more natural velocity profile is to put a bound at some position where the velocity stops growing and beyond that it stays constant, that is,

$$\Omega(x) = Cx, \quad |x| < M; \qquad \Omega(x) = \mp CM, \quad x \lessgtr \mp M.$$

For this velocity profile, the resulting scaling is intermediate between ballistic and diffusive (i.e., super-diffusive) having $1 < \gamma_y < 2$. This is because a constant flow produces a ballistic transport, meaning $\sigma_y^2 \sim n^2$, while the confined linear flow has a slower contribution. Combining this with the diffusion produced by the waves the

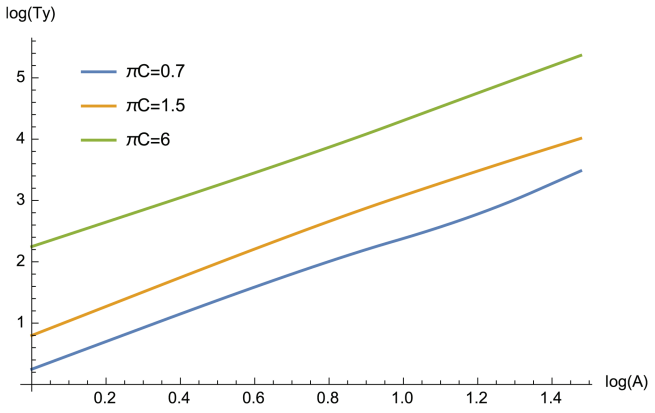

FIG. 8. Transport coefficient for a thermal distribution of Larmor radii as a function of A for $\rho_{th} = 1$ showing a quadratic dependence. The increase of the shear flow also produces an approximate quadratic increment in the value of T_y.

variance would be

$$\sigma_y^2 = 2D_y n + T_{yb} n^2. \tag{27}$$

As particles reach the constant flow region, they will be transported ballistically with the corresponding constant velocity so that, if it is large enough, the scaling would be dominated by the ballistic term. Thus, the wider the shear region ($|x| < M$) the larger the velocity and the more ballistic the transport will be ($\gamma_y \approx 2$), for a fixed time and fixed C. Also, for a given shear width, following the transport for a long enough time the scaling will be ballistic which is the dominant term.

a. FLR effects in y transport. Gyro-averaging over the Larmor radius does not change the properties described for zero Larmor

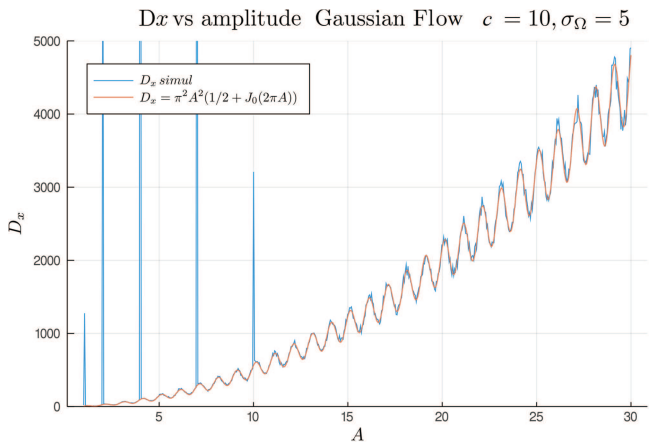

FIG. 9. Diffusion coefficient in x direction as a function of A for a Gaussian velocity profile.

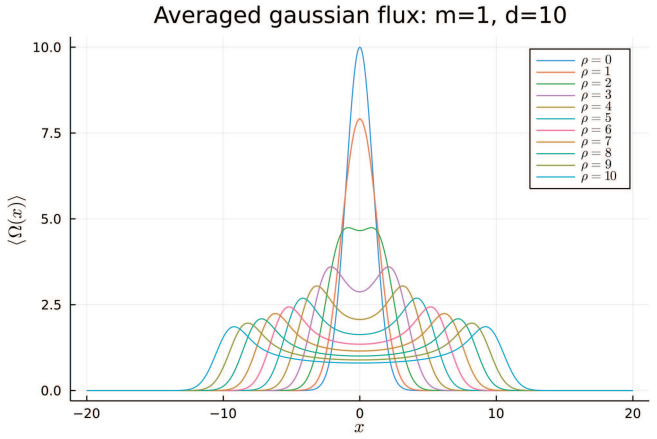

FIG. 10. Bifurcation of the Gaussian velocity profile seen by particles when gyro-averaging as ρ is increased.

radius, the sole effect being the replacement $A \to AJ_0(\sqrt{2}\rho)$. This means the transport is super-ballistic for unbounded flow and ballistic for bounded flow and with a transport coefficient that depends on the Larmor radius as $T_y \sim J_0^2(\sqrt{2}\rho)$. The PDF remains a Gaussian with the same self-similarity property [see Eq. (26)]. Only when a thermal distribution for Larmor radii is assumed, the PDF is modified to a non-Gaussian function as it was the case with no flow. This effect is most noticeable for large thermal Larmor radius ρ_{th} since for $\rho_{th} \ll 1$ the PDF is very close to a Gaussian. This has been shown in Fig. 13 of Ref. 2. The self-similarity for super-ballistic transport is now expressed as

$$P(y,t) = \frac{1}{\sqrt{T_y} t^{3/2}} \mathcal{G}_{\rho_{th}}(y/\sqrt{T_y} t^{3/2}). \tag{28}$$

The transport coefficient T_y defined in Eq. (19), after gyro-averaging and for a thermal distribution of the gyro-radius has a dependence on A and C which is shown in Fig. 8. As compared to the fixed ρ case of Eq. (24), the quadratic dependence on A is preserved, as seen by the lines with slope 2 in this log–log plot, as well as the approximately quadratic dependence on C. Thus, the scaling for T_{y1} given in Eq. (24) still holds after a thermal distribution of ρ is applied. The analytical expression can be shown to be

$$T_{y1} = \frac{4\pi^4 C^2 A^2}{3} e^{-\rho_{th}^2} I_0(\rho_{th}^2). \tag{29}$$

This indicates that large gradients in the flow are effective in increasing the super-ballistic transport rate in y direction in a thermal plasma but it is suppressed by the increase in the temperature.

B. Localized shear flow

We now consider a different type of background flow, namely a profile that is mostly localized to a plasma region of x and consequently is non-monotonic. This can be used to model zonal flows which in plasmas and fluids are known to reduce the transport creating transport barriers.[3] The resulting map is non-twist because at

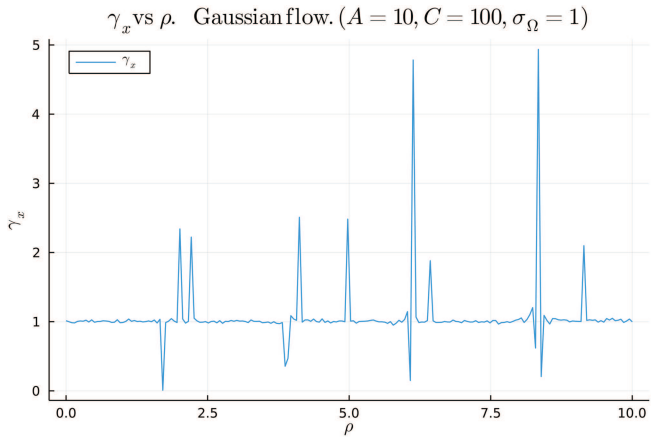

FIG. 11. Scaling exponent for transport in x direction which indicates that transport is diffusive, except for few ρ values.

the velocity maximum the velocity derivative (shear) vanishes which violates the twist condition. The shearless curve is quite robust to break up and therefore acts as a transport barrier. Rather than looking at the properties of these transport barriers, we focus here on the statistical properties of transport when global chaos is already established.

1. Gaussian velocity profile

We choose a Gaussian profile to study the transport in non-monotonic velocity shear flows. Thus, we consider

$$\Omega(x) = C\exp(-x^2/2\sigma_\Omega^2) \tag{30}$$

in the two-step mapping represented by Eq. (15) before gyro-averaging. A particular feature, in contrast with the linear flow, is that there is a net matter displacement along y because $\Omega(x)$ is always positive.

2. Transport in the x direction

As in the previous case, the transport in the x direction is diffusive, and it is affected by the flow in the y direction by decorrelating the interactions between successive iterations that give rise to the oscillations of the diffusion coefficient D_x as a function of A. However, this affects only the region where the flow is localized, so that when the particles diffuse to large x this effect will be imperceptible. Then, one can compute the diffusion coefficient D_x with the result shown in Fig. 9. It is clear that the behavior is very similar to that in Fig. 2 with no flow, confirming that the effect on suppressing the oscillations of the localized flow is negligible. Nevertheless, a distinct feature of D_x in this case is the spikes that appear at five specific points in the range $A < 10$. These are produced when there are periodic trajectories with ballistic behavior around stable fixed points with some period. Actually, they are known as accelerating modes, defined by the condition $x_\pm^{n+j} = x_\pm^n + 2\pi m_\pm$ where j is the periodicity of the mode and $m_\pm$ are integers. It can be shown that for $m_\pm = 0$, the period-2 accelerating points of the map without flow, Eq. (6), satisfy the condition

$$\pi A\sin(x_+^n) = -x_-^n + \pi n_+; \quad \pi A\sin(x_-^n) = -x_+^n + \pi n_-. \tag{31}$$

This expression can be used to numerically obtain the position of the accelerating modes. In the presence of the unidirectional flow, these points are carried away ballistically, which is reflected in the high values of D_x although D_x as a diffusion coefficient loses its meaning.

The PDF for x is Gaussian and self-similar as in the other cases.

a. FLR effects. An important feature that results when gyro-averaging the Gaussian flow is a bifurcation event that switches the flow seen by the particles from having one maximum to having two

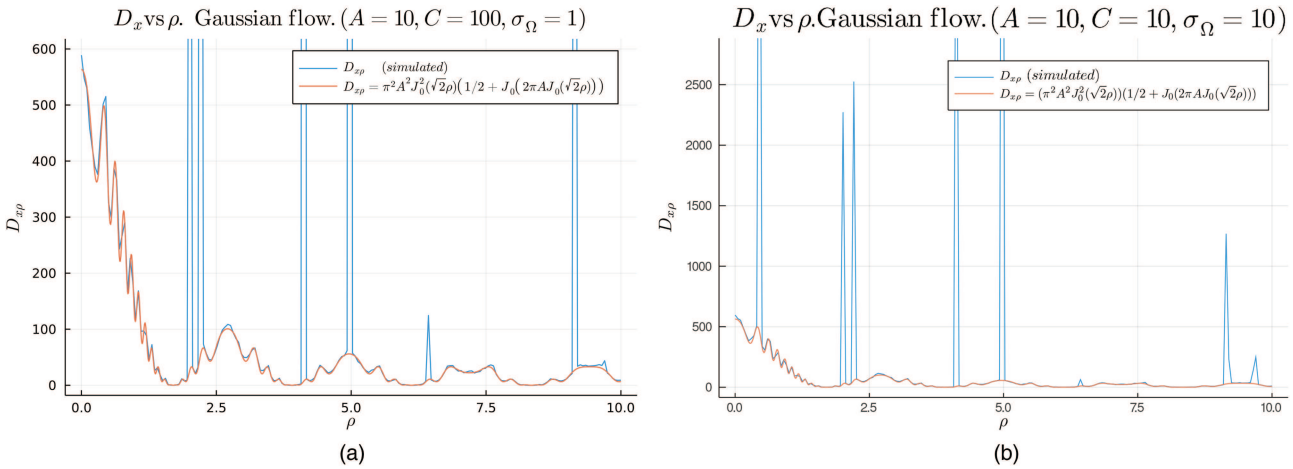

FIG. 12. Gyro-averaged diffusion coefficient for transport in x for Gaussian flows of same strength [$= C\sigma_\Omega$] (a) narrow ($C = 100, \sigma_\Omega = 1$) and (b) wide ($C = 10, \sigma_\Omega = 10$).

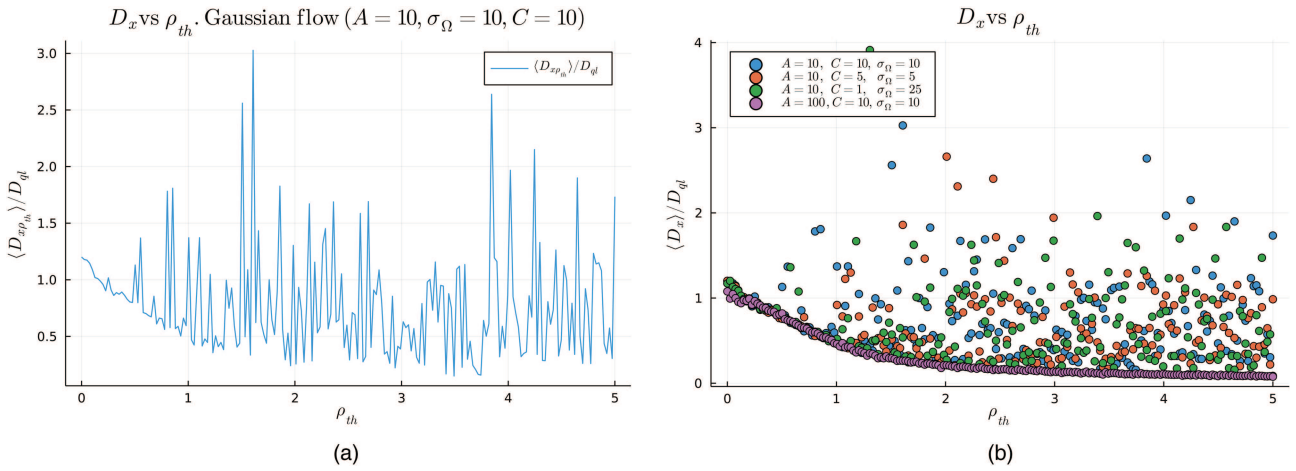

FIG. 13. Normalized diffusion coefficient for transport in x for a thermal plasma with Gaussian flow as a function of the thermal Larmor radius: (a) for a single case with $A = 10, \sigma_\Omega = 10, m = 10$ and (b) for different parameters of the Gaussian and the waves.

maxima as the Larmor radius is increased. This can be appreciated in Fig. 10 for the parameters $C = 100, \sigma_\Omega = 1$. The same bifurcation was noticed in Refs. 4 and 10 for a $\mathrm{sech}^2(x)$ velocity profile. This implies a change in the orbit topology (phase space) for $\rho > \rho_c$, where ρ_c is the bifurcation value. In the case of Fig. 10, it is 1.77.

Unfortunately, for the Gaussian flow, it is not possible to obtain the gyro-averaging analytically, and it can only be done numerically. In order to first determine if the transport is diffusive, a large number of simulations was performed and they were adjusted to the scaling of Eq. (17). It was found that $\gamma_x = 1$ except for a few especial ρ values, probably arising from the accelerating modes (see Fig. 11). With this information we can compute the diffusion coefficient. It turns out that the oscillations in $D_{x\rho}$ as function of the Larmor radius are still preserved in this case. This is shown in Fig. 12. As in the case before gyro-averaging, the spikes, presumably also due to accelerating modes, are seen too, which means that all the features are preserved when FLR effects are included. Of course, the exact results would depend on the properties of the Gaussian flow through the parameters σ_Ω and C, but for flows of the same strength, which we define as the area under the Gaussian, proportional to the product $C\sigma_\Omega$, the function $D_{x\rho}(\rho)$ is the same, which is shown in this figure too. Although there is no analytic expression to compare with, the fit to the expression with no flow is quite good still, as seen in the figure.

Now, turning to the case of a thermal distribution of ρ, the situation is more difficult to understand since the superposition of all the Larmor radii with their own singularities produces a complex mixing. The results of the numerical simulations are shown in

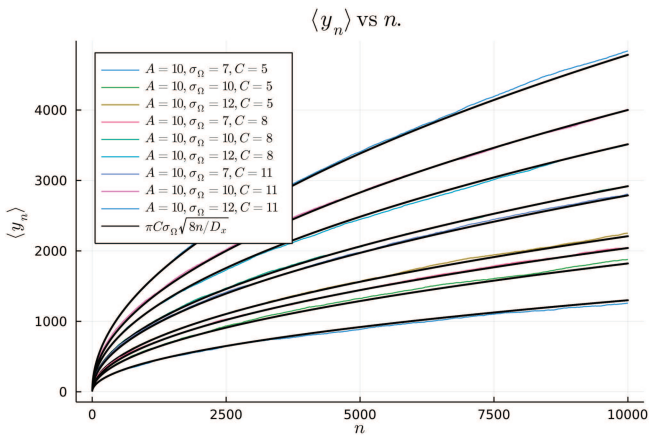

FIG. 14. Mean displacement in y produced by the simplified Gaussian map as a function of time for different parameter values.

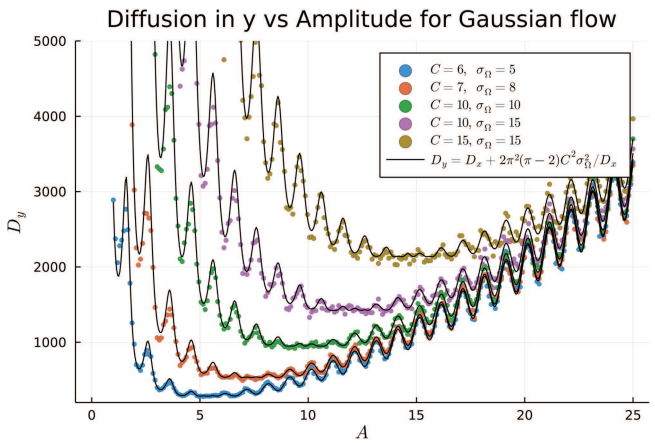

FIG. 15. Diffusion coefficient in y for a Gaussian shear flow, showing oscillations and a large increase for small A.

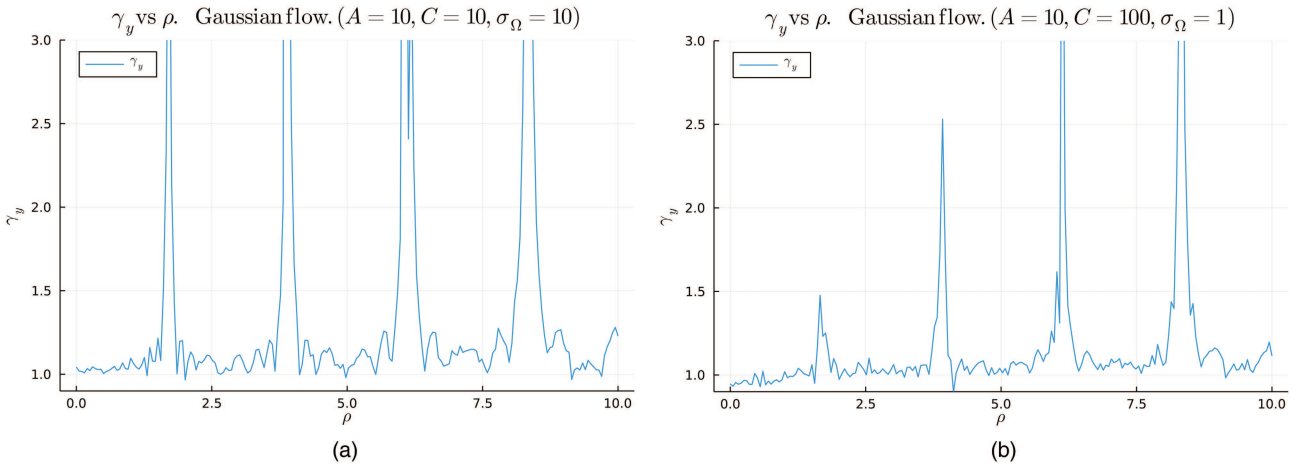

FIG. 16. Scaling exponent for gyro-averaged y transport when $A = 10$ for Gaussian flows with parameters (a) $C = 10, \sigma_\Omega = 10$, (b) $C = 1, \sigma_\Omega = 100$.

Fig. 13. Despite the mixing and wide spreading in the values of $\langle D_{x\rho}\rangle$, there is a clear underlying lower bound of the same type of the one obtained without flow in Fig. 4. Therefore, we can say that the thermal average still produces transport coefficients that on average decrease with ρ_{th} even in the presence of a zonal flow, but they have a wider range of possible values.

The probability distribution function for x transport can be obtained from Eq. (10). As expected, the same results as with no flow are obtained since the flow affects only the y transport. That is, the PDF is nearly Gaussian for small ρ_{th} but has an exponential decay for large ρ_{th}.

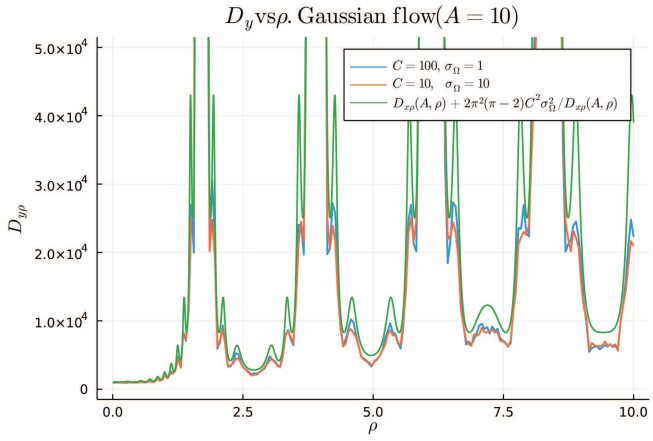

FIG. 17. Diffusion coefficient in y for gyro-averaged map as a function of ρ for a wide and a narrow Gaussian velocity profiles. It shows singularities at points given by the zeroes of $J_0(\sqrt{2}\rho)$. Comparison with analytical D_y without gyro-averaging is shown to give a fairly good match.

3. Transport in the y direction

It is expected that the localized flow would affect more the transport in the y direction. In fact, this flow produces a net displacement of an initially static ensemble of particles. The average displacement can be estimated as follows. The flow has width σ_Ω and a velocity of order C. On the other hand, the particle distribution in x has the Gaussian form $\frac{1}{\sqrt{2\pi}\sigma}e^{-x^2/2\sigma^2}$ with the diffusive behavior $\sigma^2 = 2D_x n$. Then, the fraction of particles that are subject to the action of the flow is of order $\delta N/N \approx \sigma_\Omega/\sqrt{2\pi}\sigma$ and the flow strength they feel is of order C. The average position of all the particles changes in one step by $\delta\langle y\rangle = C\delta N/N = C\frac{\sigma_\Omega}{\sqrt{4\pi D_x n}}$ which scales with time as $n^{-1/2}$. The mean displacement at time n can be found integrating over time up to step n. Thus, one finds $\langle y\rangle \approx C\frac{\sigma_\Omega}{\sqrt{\pi D_x}}\sqrt{n}$. This scales now like $\sqrt{n}$. A more accurate value, obtained from a simplified mapping like the that in Eq. (21) but for a Gaussian flow, gives for $n \gg 1$,

$$\langle y\rangle = \frac{\pi\sqrt{8}C\sigma_\Omega}{\sqrt{D_x}}\sqrt{n}. \tag{32}$$

In Fig. 14, this expression is compared with numerical results for different values of the velocity C and it shows that the match is almost perfect.

With the same simplified mapping, it is possible to find the variance $\langle y^2\rangle$, which results to be linear in time n, so transport is diffusive and the diffusion coefficient is

$$D_y = D_x + \frac{2\pi^2 C^2\sigma_\Omega^2}{D_x}(\pi - 2). \tag{33}$$

This is shown in Fig. 15 compared with numerical simulations for several parameters of the flow. It shows an interesting non-monotonic dependence with A in addition to the oscillations: it grows for both large and small A. The increase in D_y as A gets smaller, as well as the increase of $\langle y\rangle$, is due to the fact that the spread of the particle population in x is reduced, leading to a larger particle fraction feeling the localized flow. However, one should be aware

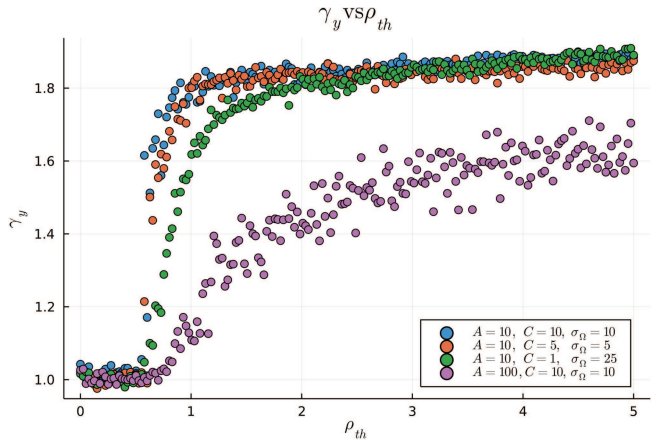

FIG. 18. Scaling exponent for thermally distributed particle y transport for Gaussian flows with different parameters and two wave amplitudes. A transition is observed for all cases.

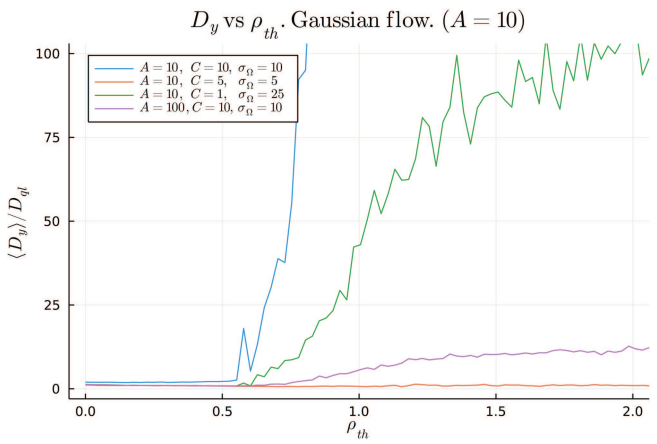

FIG. 19. Diffusion coefficient in y for thermal distribution of particles for the same parameters of Fig. 18.

that the result breaks down for very small A when the x variance drops below the flux width. In that case, all particles are dragged by the flow and no further increase would occur.

a. FLR effects in y transport. Since the gyro-averaging cannot be done analytically, all the results are again numerical when including FLR effects. The first thing to determine is the nature of transport in the presence of FLR. Fitting the simulations to the scaling for the variance of Eq. (19), it was found that the exponent varies as ρ is changed in the way of Fig. 16. One can see that it is close to 1 most of the times, and it presents the singularities already noticed in the transport in x related to accelerating modes. There are four singular values of ρ in this range, around which the transport is not diffusive but for the rest a diffusion coefficient can be computed. The behavior is the same for the two Gaussian profiles presented: wide $(C = 10, \sigma_\Omega = 10)$ and narrow $(C = 1, \sigma_\Omega = 100)$.

The diffusion coefficient obtained for the same cases is presented in Fig. 17. As we already know the transport around the four singular points in Fig. 16 is not diffusive, and hence, the large values seen here are meaningless. The figure compares the results for the two Gaussian widths, and they are quite similar. Also, they are compared with the analytical expression for the y transport in Eq. (33) obtained without FLR effects and the match is surprisingly good. This is an indication that the diffusion is not much affected by the gyro-average. It is also apparent from here that the singularities come from the zeros of the Bessel function $J_0(\sqrt{2}\rho)$ that appears in the denominator of D_y.

Now, we turn to the case of a thermal distribution of Larmor radii. We already know that when there is no flow, the thermal average modifies the properties of the PDF but the scaling with time stays diffusive. In order to find out whether or not the localized flow changes, the transport scaling, we computed the exponent γ_y for this case and plotted it as a function of the thermal gyro-radius in Fig. 18. This plot contains the results for different Gaussian shapes and wave amplitudes and for all of them there is the interesting property of a transition in the value of γ_y from one to $\gamma_y > 1$. When the amplitude is $A = 10$, the transition is at about the same value of $\rho_{th} \approx 0.5$ for all the profiles, jumping to $\gamma_y \approx 1.9$. The transport becomes very super-diffusive nearing the ballistic scaling, as a result of the flow. However, for the large wave amplitude $A = 100$, the transition is retarded and γ_y does not grow so fast; the transport is not so super-diffusive. This is due to the increased chaos, which tends to lessen the effect of the background flow.

The diffusion coefficient for a thermal distribution can be seen in Fig. 19 as a function of the thermal Larmor radius. The same transition observed for γ_y is evident here, although this is to be expected because for non-diffusive transport, the diffusion coefficient loses its meaning and, when computed, gives large values.

Finally, it is of interest to know whether the particle distribution function type is affected by the thermally distributed Larmor radii in the same way as in the case without flow. This time, since there is a net particle displacement, the centroid of the PDF should have a displacement as time evolves, which scales as $\sqrt{t}$, according to Eq. (32). Also, the net flow in the positive y direction would break the symmetry leading to larger particle accumulation on the right side of the peak than on the left side. This can be appreciated in Fig. 20 where the PDF in the y direction is shown for both small (< 1) and large (> 1) ρ_{th}. Panel (a) depicts the PDF relative to the centroid position for the normalized variable y/σ_Ω for $\rho_{th} < 1$ and shows a slight displacement of the centroid relative to the maximum implying a longer tail on the right hand side of the peak, while panel (b) illustrates that for $\rho_{th} > 1$, the longer right tails are more evident. It also shows that for the later times (more iterations) the PDF gets wider and shorter when ρ_{th} is large, which would be expected from a net directed flow. The plots show that for small ρ_{th} there is almost no dependence on ρ_{th} while for larger ρ_{th} the PDF has a larger asymmetry and shows the presence of some ballistic particles. These are the smaller peaks on the right hand tail, corresponding to different velocities. In Fig. 20(a), a slight non-Gaussian shape can be noticed (the Gaussian is shown for comparison).

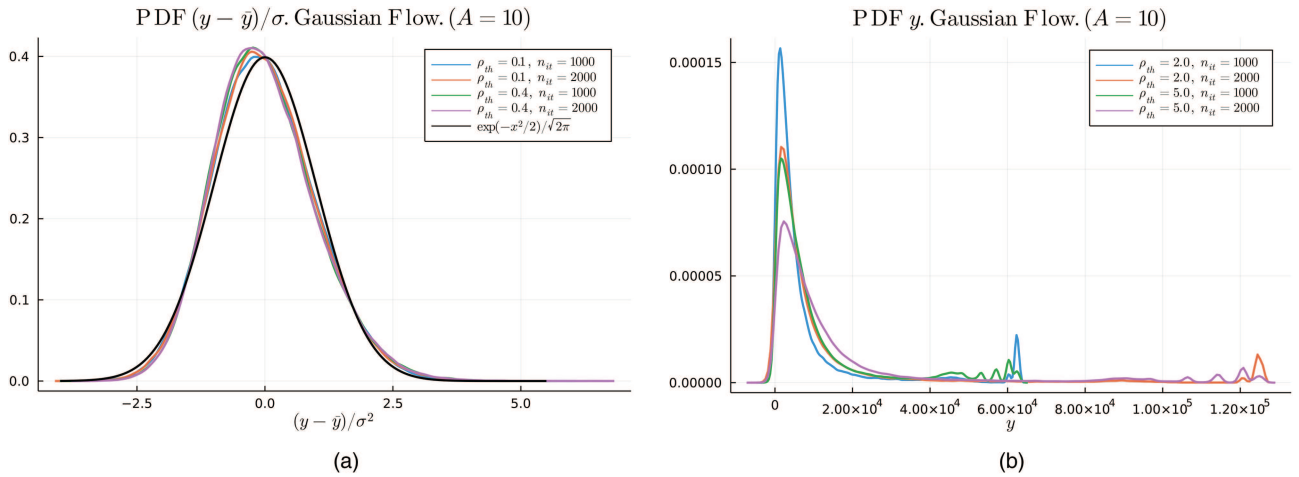

FIG. 20. PDF for localized flow for varying thermal Larmor radius and time (iterations) when $\rho_{th} < 1$ (a) and $\rho_{th} > 1$ (b). The time evolution shows the net displacement of the centroid of the PDF and the left–right asymmetry, primarily for large ρ_{th} in (b). Here, $A = 10$ and $C = 10$.

On the other hand, for large ρ_{th}, departure from Gaussianity is not so easy to identify due to the intrinsic large asymmetry. In order to have a better appreciation of the PDF features, we take advantage of the fact found before that the PDF has self-similar properties and those depend on the type of transport. So, for diffusive transport, the self-similar relation of the type in Eq. (14) applies, while for ballistic transport, one would expect a self-similarity scaling of the type

$$P(x,t) = \frac{1}{\sqrt{T_y t}}\mathscr{G}_{\rho_{th}}(y/\sqrt{T_y t}). \tag{34}$$

Thus, in Fig. 21, we plot normalized PDFs in log-scale for the two cases: diffusive in (a) and ballistic in (b). It is clear from panel (a) that the PDFs for all times collapse to a single self-similar function except for the far tails that correspond to the ballistic particles. It is also evident that the fall-off of the distribution tend to straight lines on both sides implying an exponential decay of the tails as opposed to the Gaussian tails. Then, for $\rho_{th} > 1$, the non-Gaussian PDF property is preserved from the case with no flow. In panel (b), one can see that the ballistic scaling fits the spikes on the tails, for all times, confirming the ballistic nature of these particles.

V. SUMMARY AND CONCLUSIONS

Turbulent transport in magnetized plasmas due to a discrete spectrum of drift waves in two dimensions can be studied as the chaotic transport in a symplectic mapping. We used Cartesian coordinates in 2D, but it can be applied to a tokamak plasma in the

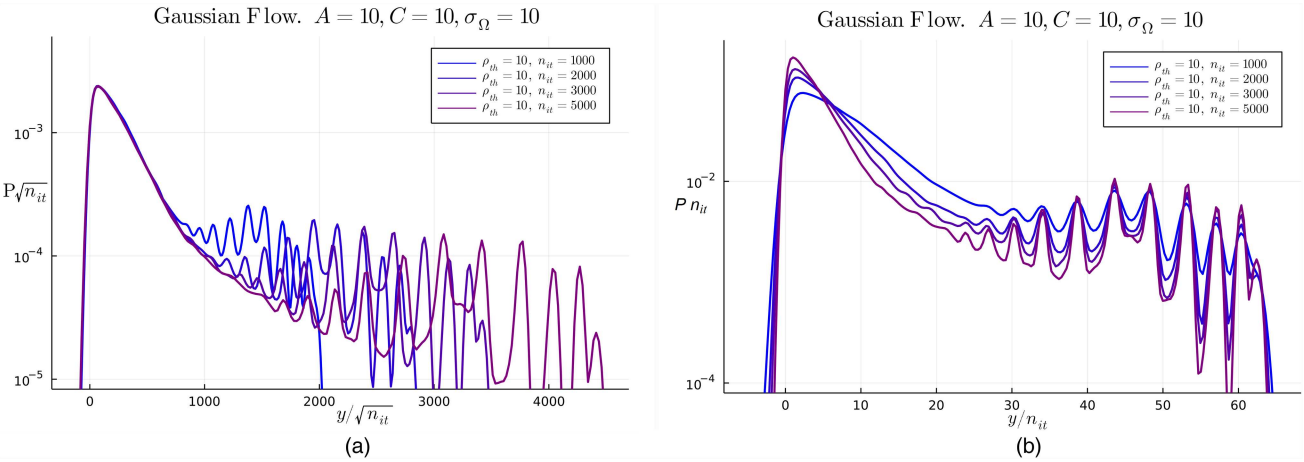

FIG. 21. PDF in the log scale for non-monotonic flow for various times n_{it} using (a) the self-similar diffusive scaling $\sqrt{n_{it}}P$ vs $y/\sqrt{n_{it}}$ and (b) the self-similar ballistic scaling tP vs y/t, for the parameters $A = 10$, $C = 10$, $\rho_{th} = 10$.

poloidal plane identifying the radial and poloidal coordinates with x and y axes, respectively. Inclusion of poloidal sheared flows has the effect of yielding a twist map if the flow is monotonic and a non-twist map when it is non-monotonic. The chosen wave spectrum has been used previously in Ref. 1 to study the phase-space orbits and some statistical properties of transport and in Ref. 2 to include FLR effects. Non-local transport may result when the particles have a thermal distribution of FLR, which shows up as a non-Gaussian PDF. In the present study, we extended the analysis to the case with non-monotonic shear flow in addition to the monotonic flow studied earlier. We also studied the properties of the transport for all relevant cases in some detail.

Background flows modify the particle dynamics changing in turn the chaotic properties that produce the transport. A large poloidal shear flow drags the particles along the poloidal direction, hindering the chaotic motion produced by the waves. When there is chaos reduction in some region due to a localized flow, there can be a surface where regular motion is restored and this is identified with a transport barrier. However, we focused here on the case when global chaos is maintained even in the presence of flow and considered the resulting modification of transport.

When no flow is present, we obtained the diffusive transport and recovered the well-known quasilinear diffusion coefficient that scales with the wave amplitude as A^2 and presents oscillations due to coupling between successive steps.[7] In addition, the PDF is Gaussian and self-similar. When FLR effects are included, the diffusion coefficient D presents oscillations as a function of ρ with a double period. For a realistic plasma, the particle Larmor radius should have a thermal distribution and when this is included, D is a decreasing function of the thermal gyro-radius ρ_{th}, which implies that transport is reduced for hotter plasmas. Also, the PDF becomes non-Gaussian when ρ_{th} is large enough, remaining self-similar. This means that FLR effects give rise to non-local transport since particles sample wider regions in their orbits.

Inclusion of a background flow requires the process to be described by a two-step mapping. This makes it more difficult to analyze the transport properties and for that reason, we considered simplified maps that preserve the essential features of the original one but allow us to get analytical results and understand the underlying cause for the observed scalings of transport. Transport in the two directions has now to be studied separately. In the x (radial) direction, we showed that the transport is still diffusive, and non-local for thermally distributed Larmor radii, as in the case without flow, independently of the type of flow profile. However, in the y (poloidal) direction, transport is modified differently depending on the type of flow. For a linear shear flow profile, it becomes super-ballistic since the flow velocity keeps increasing as particles go to larger x. By bounding the flow growth to a finite region, super-diffusive transport results. For a localized flow, due to its limited action range, it stays diffusive mostly, but it can be super-diffusive when the thermal distribution of particles is included. It is worth mentioning, though, that the poloidal transport has no effect on the confinement and, therefore, it has no direct relevance for fusion experiments.

For the two types of shear flows considered, the transport coefficients have the following features: (1) for monotonic profile, (a) D_x no longer has oscillations with A following the quasilinear value, and it is smaller than the flowless D_x. As a function of ρ, the coefficient D_x oscillates with a single period ($\sim A^2 J_0^2(\sqrt{2}\rho)$). The PDF is Gaussian but for a thermal distribution of FLR it becomes non-Gaussian for $\rho_{th} > 1$ and is self-similar. (b) The transport in the y direction is not diffusive [the variance is given by Eq. (25)]; the transport coefficient scales quadratically with A and the flow strength C. The PDF is Gaussian with its width scaling as t^3. When the growth of linear flow is bounded, the variance is given by Eq. (27). Including FLR effects, the scalings with A and C stay the same and oscillations with ρ are present as before. For a thermal distribution, the scalings are not modified and the PDF is becomes non-Gaussian with a self-similar structure.

(2) For non-monotonic flow profile, (a) D_x maintains the oscillations with A and singular points appear associated with accelerating modes. It has the double period oscillations as a function of ρ, but it has a uniform decrease with ρ_{th} for a thermal plasma. (b) In the y direction, there is a net displacement that grows as the square root of time. The transport is diffusive and the diffusion coefficient D_y [given by Eq. (33)] has the oscillatory behavior with A and increases drastically for low A. This is obtained also in numerical computations. The inverse dependence with D_x produces that the dependence with ρ has singularities at the zeros of $J_0(\sqrt{2}\rho)$; around these singular points, the transport is not diffusive. The interesting feature is that for thermal distribution of FLR, the transport is super-diffusive when ρ_{th} is larger than a threshold value (about $\rho_{th} \approx 0.5$ for $A = 10$). On the other hand, the PDF is asymmetric with a longer tail in the direction of the flow and some ballistic particles are present. For the thermal plasma, it also becomes non-Gaussian for $\rho_{th} > 1$.

ACKNOWLEDGMENTS

This work was supported by Project Nos. DGAPA-UNAM IN110021 and IN110021, Conacyt Project No. A1-S-24157, and supercomputer Project No. LANCAD-UNAM-DGTIC-104.

AUTHOR DECLARATIONS

Conflict of Interest

The authors have no conflicts to disclose.

Author Contributions

Jorge Torres: Conceptualization (equal); Formal analysis (equal); Investigation (equal); Software (equal); Writing – original draft (supporting). **Julio J. Martinell:** Conceptualization (equal); Formal analysis (equal); Investigation (equal); Software (equal); Writing – original draft (lead).

DATA AVAILABILITY

The data that support the findings of this study are available within the article and shown in the figures.

REFERENCES

[1] R. Kleva and J. Drake, Phys. Fluids **27**, 1686 (1984).
[2] N. Kryukov, J. Martinell, and D. del Castillo-Negrete, J. Plasma Phys. **84**, 905840301 (2018).

[3]D. del Castillo-Negrete, Phys. Plasmas **7**, 1702 (2000).
[4]J. Martinell and D. del Castillo-Negrete, Phys. Plasmas **20**, 022303 (2013).
[5]D. del Castillo-Negrete and P. Morrison, Phys. Fluids A **5**, 948 (1993).
[6]C. Karney, Phys. Fluids **22**, 2188 (1979).
[7]T. Antonsen and E. Ott, Phys. Fluids **24**, 1635 (1981).
[8]A. Lichtenberg and M. Lieberman, *Regular and Chaotic Dynamics*, 2nd ed. (Springer, 1992).
[9]C. Tafoya and J. Martinell, Radiat. Effects Def. Solids **177**, 124 (2022).
[10]D. del Castillo-Negrete and J. Martinell, Comm. Nonlinear Sci. Numer. Simulat. **17**, 2031 (2012).